Interferometric readout for tiltmeter

Fabián Erasmo Peña Arellano

Abstract

The design and characterization of a Michelson interferometer for the readout of a precision tiltmeter is reported. A collimator is designed with Zemax for the case in which the laser is taken to the interferometer using a fibre. The maximum angular displacement of the tiltmeter that the interferometer can tolerate is calculated. The noise produced by the transimpedance amplifier of the photodiode is calculated and compared with experimental measurements. The contributions of displacement noise, laser intensity noise, acoustic noise and ground vibrations are experimentally identified. The effects of feedback when the laser cavity is coupled to the optic fibre are also pointed out.

I. INTRODUCTION

The aim of this report is to identify the noise sources limiting the performance of a Michelson interferometer, intended as a readout instrument for an advanced tiltmeter. Currently, the tiltmeter is using as readout a couple of linear variable differential transformers (LVDT), which provide a sensitivity of $9\times10^{-11}\,rad/\sqrt{Hz}$ [1]. Such an amount of sensitivity is enough for the task the tiltmeter is intended to perform. The interferometer is rather a tool for testing advanced wedges and the elastic properties of new materials that would improve the ultimate performance of the tiltmeter rather than a substitute of the LVDT's.

As will be shown in section V (figure 7), the interferometer is currently limited by laser intensity and ground vibrations noise, with a noise floor of $4.5\times10^{-14}\,rad/\sqrt{Hz}$. Section II describes the collimator used for taking the laser into the interferometer when an optic fibre was employed. In section III the angular range of the interferometer is calculated. The readout of the transimpedance amplifier is described in section IV. In section V the noise sources limiting the sensitivity of the interferometer are described.

II. COLLIMATION OF THE BEAM

In order to achieve an optimum performance of the interferometer, the incoming beam must be appropriately collimated. The quality of the beam does not only depend on the amount of defocus, but it is also determined by the amount of the aberrations when a lens is used. Both, defocus and any type of aberration, can be described in terms of an optical path length difference (OPLD) between a ray and the reference ray, which in this design is the principal ray, shown in black in figure $1(a)$. Such an OPLD varies along the cross section of the beam, and it must be minimized, with an appropriate optimization procedure, in order to produce good quality interference fringes with the interferometer.

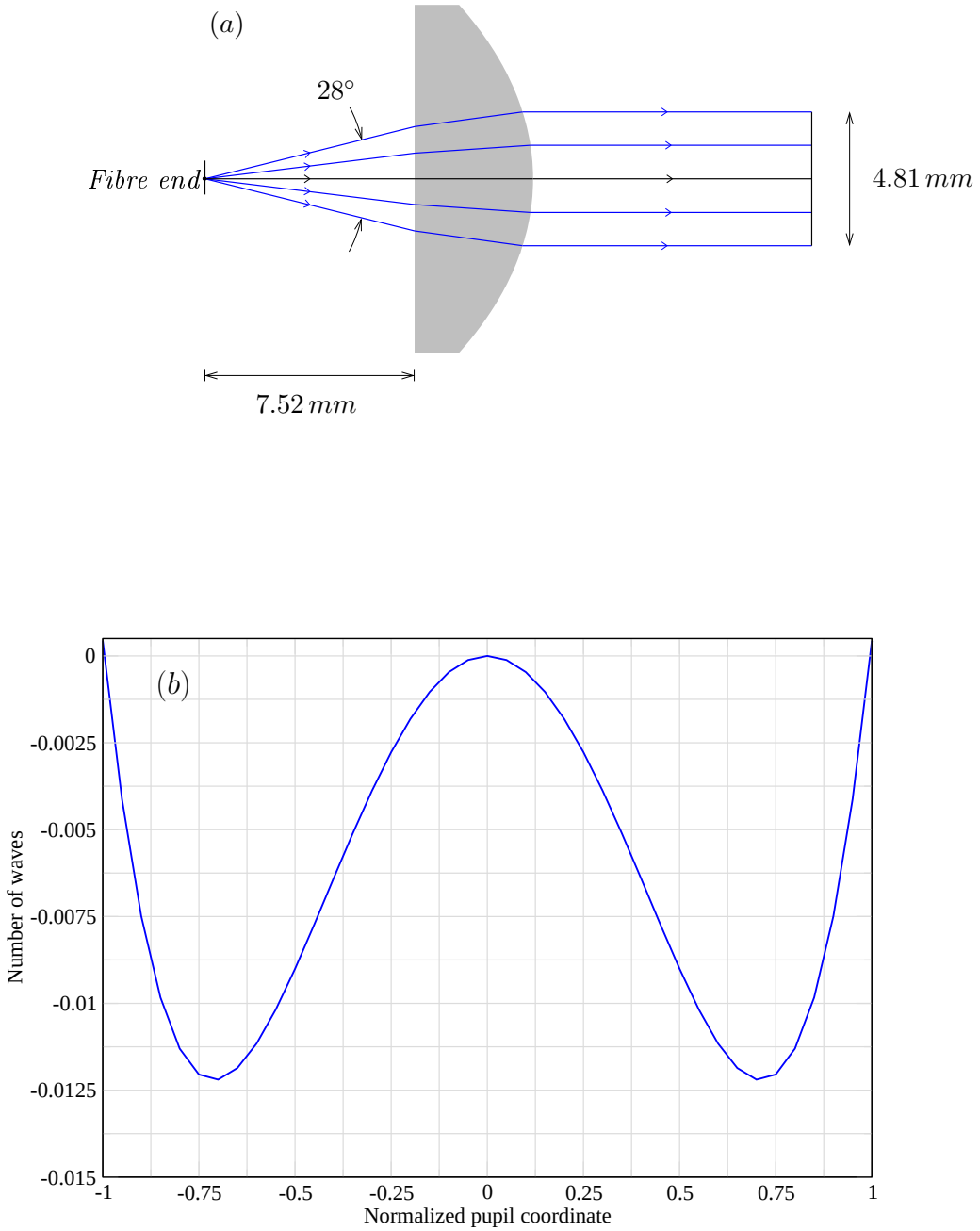

Figure 1: A diffraction limited collimated beam is achieved with an aspheric lens. The collimator layout is shown in (a) and the optical path length difference with respect to the chief ray as a function of the exit pupil coordinate is shown in (b). The exit pupil is $4.81\,mm$ in diameter.

Although there are collimators commercially available, experience with these devices in developing the optical lever for Advanced LIGO [1] suggests that it is a good approach to design and assemble a collimator to produce a large diameter beam in order to fit the purposes of the interferometer. Although the interferometer is going to be intensity locked to a fixed phase and angular position, a larger diameter provides a larger angular range over which the two beams interfere meaningfully. As will be seen in section III, a diameter of approximately $4.81\,mm$ theoretically provides an angular range of $3.97\,mrad$, which is more than the mechanical range of the tiltmeter arm. For Figure 1(a) shows the layout of the collimator modeled with Zemax. The diameter of the core of the single mode fibre is neglected and it is assumed that the light diverges from a point source. The divergence of the light from the point source is approximately 28° full span. This value was estimated from the size of a collimated beam that a lens with a known focal length produced. The collimation was achieved by visual inspection. The distance between the fibre end and the lens was adjusted until the diameter of the beam remained approximately constant over few meters. For this task it was not necessary a diffraction limited beam. The lens shown in the diagram (a) is the aspheric lens $AL1210$ from Thorlabs. The calculated OPLD of the wavefront as a function of the exit pupil is shown in figure 1(b). It is a lot smaller than a quarter of a wavelength.

The lens and the fibre end were mounted in a cage system whose geometry constrains these two components to be aligned to some extent. The holders provide coarse adjustment for the distance between the lens and the fibre end (z-direction), and also for the position of the fibre end in a plane perpendicular to the direction of the propagation of the light ($x-$ and $y-$directions).

Visibilities of the interference pattern of approximately 97% were achieved, in practice, the collimation of the beam requires additional work. Experience suggests that control of tip and tilt of the fibre end may also be necessary. As seen on a

screen, the beam does have some features that break the axial symmetry expected and do not disappear by translating the fibre end on the xy plane. It is also necessary to adjust the orientation of the collimator as a whole with respect to the interferometer since, currently, the central beam splitter does not have any adjustment. In order to provide such an adjustment, the collimator had to be mounted separately from the cage assembly and for this reason the mechanical design should be reviewed.

With respect to the quality of the beam, only visual inspection has been used and no quantitative assessment has been carried out. Although this method does yield, to some extent, acceptable results and does not demand additional resources, when the aim is to achieve the quality that commercial collimators may provide, a shearing plate can be used [4]. A shearing plate produces interference fringes between two samples of a single beam. Upon reflection on a slightly tilted surface, a shearing is introduced into one of the samples, and thus, straight fringes are produced. It is possible to quantify the amount of divergence of the beam by analyzing these fringes.

III. ANGULAR RANGE

Figure 2 shows a simplified diagram of the interferometer and its function as the tiltmeter readout. The main beam, incoming perpendicular to the drawing plane, is divided at point O by a beam splitter into the arms of the interferometer. Each arm is then reflected onto its own target mirror on the tiltmeter arm. As the target mirror tilts, the beams are misaligned by twice the tilt angle. As can be seen in the diagram, the beams will move in opposite directions on the beam splitter plane.

Upon interference, the tilt will produce straight fringes on the detector plane rather than circular patterns. The straight fringes will become narrower as the tilt

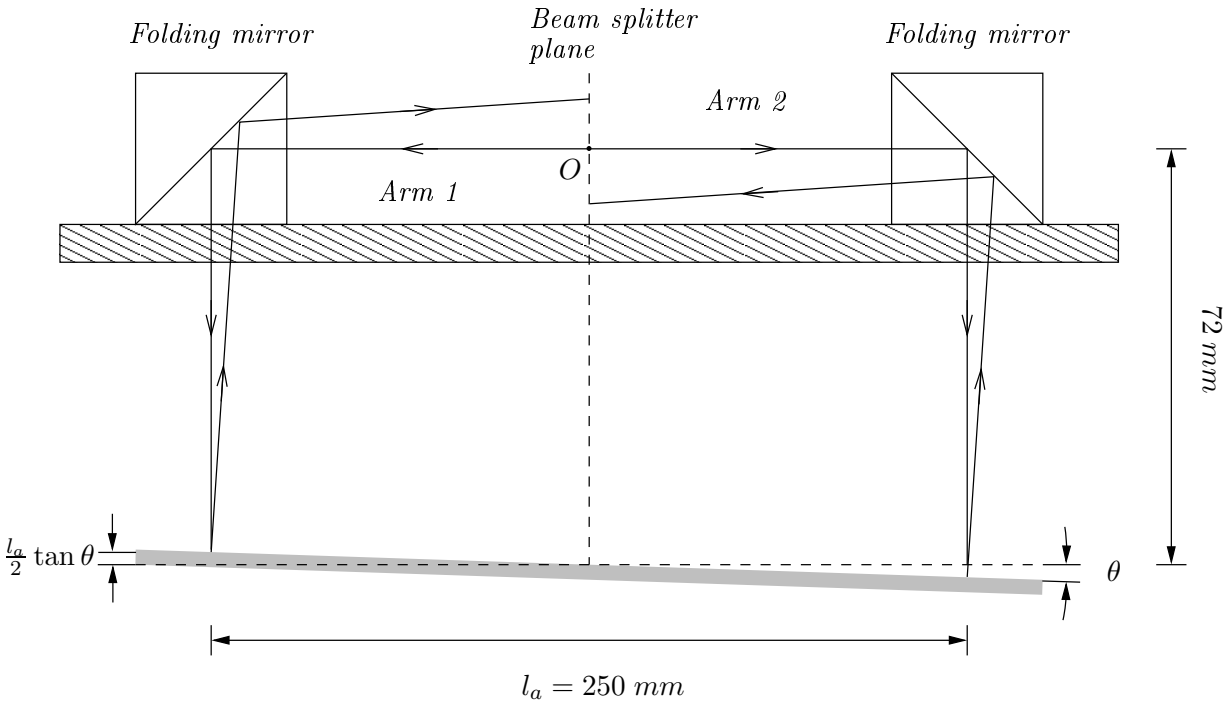

Figure 2: As the target mirrors tilt, the beams move in opposite directions on the beam splitter plane.

increases compromising the visibility of the interference pattern on the photodiode. This is a minor issue since the interferometer will be locked near to a position where the tilt is null and the fringes revert to a circular pattern. It is convenient, nevertheless, to calculate the maximum tilt which does not severely compromise the visibility. The visibility will be satisfactory as long as the thickness of the fringes is larger than the width of the overlapping area of the two beams on the detector. Figure 3 shows the principal ray of each beam propagating away from the target mirror onto the plane of the detector where the interference takes place. The electric field vectors for each beam on such a plane can be written as

$$E_1 = A\exp\left(\boldsymbol{k_1}\cdot\boldsymbol{r_1}\right), \quad E_2 = A\exp\left(\boldsymbol{k_2}\cdot\boldsymbol{r_2}\right), \tag{1}$$

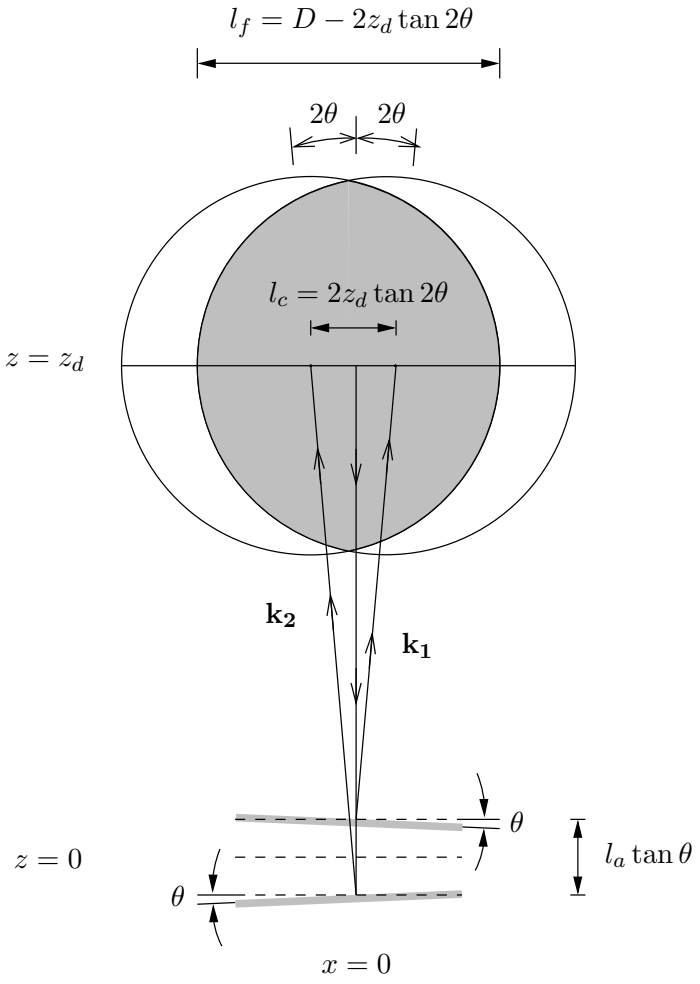

Figure 3: The width of the straight fringes should not be smaller that the width of the overlapping area of the beams on the photodiode plane.

where the wave vectors $\boldsymbol{k_1}$ and $\boldsymbol{k_2}$ are given by

$$\boldsymbol{k_1} = k \begin{pmatrix} \sin 2\theta \\ \cos 2\theta \end{pmatrix}, \quad \boldsymbol{k_2} = k \begin{pmatrix} -\sin 2\theta \\ \cos 2\theta \end{pmatrix}, \tag{2}$$

and the displacement vectors $\boldsymbol{r_1}$ and $\boldsymbol{r_2}$ are written as

$$\boldsymbol{r_1} = \begin{pmatrix} x \\ z - l_a \tan\theta \end{pmatrix}, \quad \boldsymbol{r_2} = \begin{pmatrix} x \\ z + l_a \tan\theta \end{pmatrix}, \tag{3}$$

where the contributions of both the outgoing and incoming path lengths have been taken into account. As can be seen in the diagram, the horizontal and vertical axes are referred to as x and z respectively. The origin of the reference system is at the reflection point on the target mirror when the angular displacement is zero.

The intensity of the interference pattern is calculated as

$$\begin{aligned} I &= (E_1 + E_2)(E_1^* + E_2^*) && (4) \\ &= 2A^2\{1 + \cos[2k(x\sin 2\theta - l_a \tan\theta \cos 2\theta)]\}. && (5) \end{aligned}$$

From expression (5), the thickness Δx of the straight fringes can calculated by setting the equation

$$2k\Delta x \sin 2\theta = 2\pi, \tag{6}$$

which, by introducing the value $k = 2\pi/\lambda$, can be written as

$$\Delta x = \frac{\lambda}{2\sin 2\theta}. \tag{7}$$

The maximum angular displacement can be calculated by solving the equation $\Delta x = l_f$, where l_f is the width of the overlapping area. In terms of the angular displacement θ, the diameter of the beam D and the distance z_d from the mirror to the detector, the equation is

$$2(D - 2z_d \tan 2\theta_m)\sin 2\theta_m - \lambda = 0. \tag{8}$$

For a diameter $D = 4.81\,\text{mm}$, a distance $z_d = 30\,\text{cm}$ and a wavelength $\lambda = 632.8\,\text{nm}$, the maximum displacement is $\theta_m = 3.97\times10^{-3}$ rad $= 0.22°$ one way only. This corresponds to a linear displacement of approximately $\theta_m l_a/2 = 0.496$ mm, which is within the endstops limiting the movement of the arms. The tiltmeter will be locked within 1% of the maximum displacement around the place where the arm lengths are equal. The fringe width will not be a problem in the tiltmeter readout throughout its mechanical range.

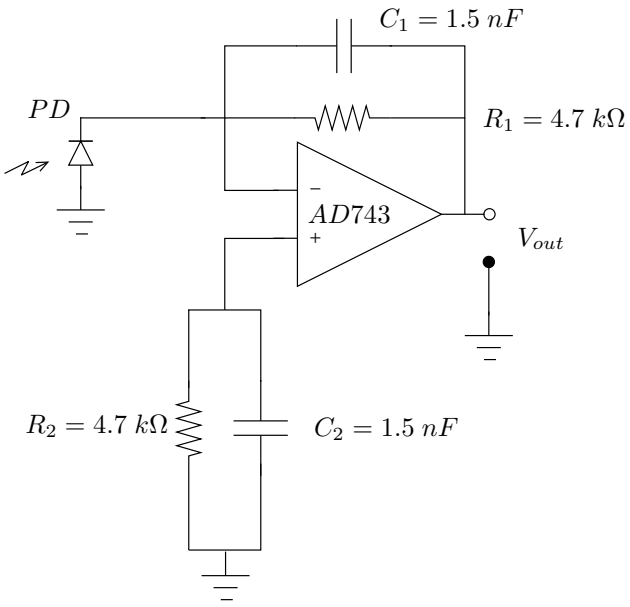

Figure 4: The transimpedance amplifier in photovoltaic mode.

IV. THE PHOTODIODE READOUT

Figure 4 shows the model of the transimpedance amplifier used as the photodiode readout. The photodiode is connected to the amplifier in photovoltaic configuration without a reverse bias. The advantage of this arrangement is that it produces a more stable dark current with respect to the unbiased mode and, therefore, there is less noise present in the system at high frequencies. The dark current is produced by the reverse bias producing a current flowing through the photodiode, which has a resistive component, even when there is no incident light. In the case of the photodiode $FDS1010$ from Thorlabs, the dark current is $600\,nA$ when a bias of $5\,V$ is applied. Applying a voltage to the photodiode does reduce its capacitance, thus increasing the reaction time of the photodiode. However, that is not a real advantage at low frequencies.

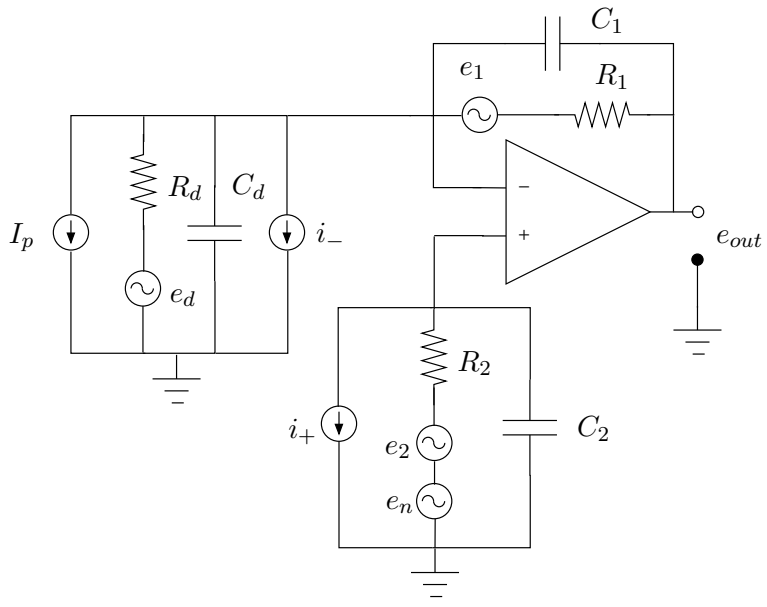

Figure 5: Noise model of the transimpedance amplifier.

The output of the amplifier is given by

$$|V_{out}| = \frac{R_1 |I_p|}{\sqrt{1 + \omega^2 R_1^2 C_1^2}}, \tag{9}$$

where R_1 and C_1 are the resistance and capacitance in the feedback branch respectively, and ω and I_p are the angular frequency of the signal and the photocurrent produced in the photodiode respectively. Figure 5 shows the noise model of the transimpedance amplifier and photodiode shown in figure 4. The parameters R_d and C_d are the resistance and capacitance of the photodiode, which in this case is the $FDS1010$ sold by Thorlabs in the package $SM1PD1A$. The voltage source $e_d = \sqrt{4kTR_d}$ is the thermal noise produced by the resistor R_d and i_d is the photocurrent produce by the interference pattern shining the photodiode, where k is Boltzmann's constant and T is the temperature of the resistor. The sources i_+, i_- and e_n are the current and voltage noise of the operational amplifier. Finally, the sources $e_1 = \sqrt{4kTR_1}$ and $e_2 = \sqrt{4kTR_2}$ are the thermal noise produced by the resistors R_1 and R_2.

Thermal noise e_1 from the feedback resistor R_1. Since the impedance in the feedback branch is

$$|z_f| = \frac{R_1}{\sqrt{1+\omega^2 R_1^2 C_1^2}} \tag{10}$$

and the inverting terminal is virtual ground, the noise $e_1 = \sqrt{4kTR_1}$ produced by resistor R_1 in the feedback branch becomes, at the output terminal

$$e_{out,1}^2 = \frac{4kTR_1}{1+\omega^2 R_1^2 C_1^2}. \tag{11}$$

Current noise i_-. Due to the large impedances of the resistance $R_d\,(> 1\,G\Omega)$ and capacitance $C_d\,(= 375\,pF)$ of the photodiode at low frequencies, these components do not draw any current, and all the current noise i_- flows to the output terminal through the feedback branch, yielding the output voltage

$$e_{out,-}^2 = |z_f|^2\, i_-^2 = \left(\frac{R_1^2}{1+\omega^2 R_1^2 C_1^2}\right) i_-^2. \tag{12}$$

Thermal noise from the resistance R_d of the photodiode. The input voltage produced by the noise source $e_d = \sqrt{4kTR_d}$ at the negative terminal of the operational amplifier is

$$|v_d| = \frac{e_d}{\sqrt{1+\omega^2 R_d^2 C_d^2}} \tag{13}$$

and the impedance of the resistor R_d and capacitor C_d in parallel can be written as

$$|z_d| = \frac{R_d}{\sqrt{1+\omega^2 R_d^2 C_d^2}}. \tag{14}$$

The output thermal noise produced by the resistance R_d then becomes

$$e_{out,D}^2 = \left|\frac{z_f}{z_d}\right|^2 |v_d|^2 = \frac{R_1}{R_D}\left(\frac{4kTR_1}{1+\omega^2 R_1^2 C_1^2}\right). \tag{15}$$

Notice that the larger the resistance R_d is, the less thermal noise will reach the output. Furthermore, since $R_D \gg R_1$ (see table I) the contribution to the noise from the feedback resistor given by expression (11) will be a lot larger than the one described by the formula (15).

Shot noise. Another source of noise going into the inverting input is the shot noise. The incoming light onto the photodiode produces a current that is affected by shot noise. In the case in which a bias voltage is applied to the photodiode, the dark current is also affected by shot noise. The output noise is easily written as

$$e_{out,shot}^2 = |z_f|^2 \left[2q\left(|I_p| + |I_d|\right)\right] = \left(\frac{R_1^2}{1+\omega^2 R_1^2 C_1^2}\right)\left[2q\left(|I_p| + |I_d|\right)\right], \quad (16)$$

where q is the charge of the electron, I_p the photocurrent and I_d is the dark current ($600\,nA$ for $5\,V$ bias voltage).

Voltage noise $\mathbf{e_n}$. The operational amplifier produces a voltage noise e_n which is placed at the non-inverting terminal. By considering that the voltage in the inverting terminal is the same as that in the non-inverting one, it is possible to show that the output noise is

$$e_{out,n}^2 = \left(\frac{e_n^2}{1+\omega^2 R_2^2 C_2^2}\right)\left(1 + \frac{R_1}{R_d}\sqrt{\frac{1+\omega^2 R_d^2 C_d^2}{1+\omega^2 R_1^2 C_1^2}}\right)^2. \quad (17)$$

Thermal noise from the resistor $\mathbf{R_2}$. Analogously, the output thermal noise from the resistor R_2 can be written as

$$e_{out,2}^2 = \left(\frac{4kTR_2}{1+\omega^2 R_2^2 C_2^2}\right)\left(1 + \frac{R_1}{R_d}\sqrt{\frac{1+\omega^2 R_d^2 C_d^2}{1+\omega^2 R_1^2 C_1^2}}\right)^2. \quad (18)$$

Current noise $\mathbf{i_+}$. Finally, the non-inverting terminal current noise is

$$e_{out,+}^2 = \left(\frac{i_+^2 R_2^2}{1+\omega^2 R_2^2 C_2^2}\right)\left(1 + \frac{R_1}{R_d}\sqrt{\frac{1+\omega^2 R_d^2 C_d^2}{1+\omega^2 R_1^2 C_1^2}}\right)^2. \quad (19)$$

The total output noise is calculated by adding all the contributions in quadrature.

Table I shows the values of the components of the transimpedance amplifier used

Component	Value
R_1	$4.7\,k\Omega$
C_1	$1.5\,nF$
R_d	$1\,G\Omega$
C_d	$375\,pF$
R_2	$4.7\,k\Omega$
C_2	$1.5\,nF$
I_d	$600\,nA$

Table I: Values of the components of the transimpedance amplifier. The values of the resistance R_D, the capacitance C_D and dark current I_d correspond to the $FDS1010$ photodiode from Thorlabs.

to calculate the total output noise. The data-sheet for the AD743 provides current and voltage noise measurements from 1 Hz up to 10 kHz. In order to predict the output noise in the frequency range of miliHertz, the $1/f$ noise behaviour was extrapolated by means of a linear least-square fit to the existing data above 1 Hz. Figure 6 shows in black the measured dark current and readout noise. The noise produced by the signal analyzer is shown in red. The addition in quadrature of the predicted noise and the noise of the signal analyzer is shown in blue. At frequencies above 100 Hz the prediction and the measurement are similar in value. In the $1/f$ regime, however, the noise from the signal analyzer continuously increases until it dominates over the predicted value, making the comparison between the prediction and the measurement meaningless.

It is important to note that a bias voltage applied to the photodiode could decrease the noise at low frequencies. The bias voltage produces an electric field across the photodiode, and this electric field imposes an order to the electrons of the photocurrent since it is in magnitude a lot larger than the local fluctuations produced by the electrons themselves. In the absence of the bias voltage, the

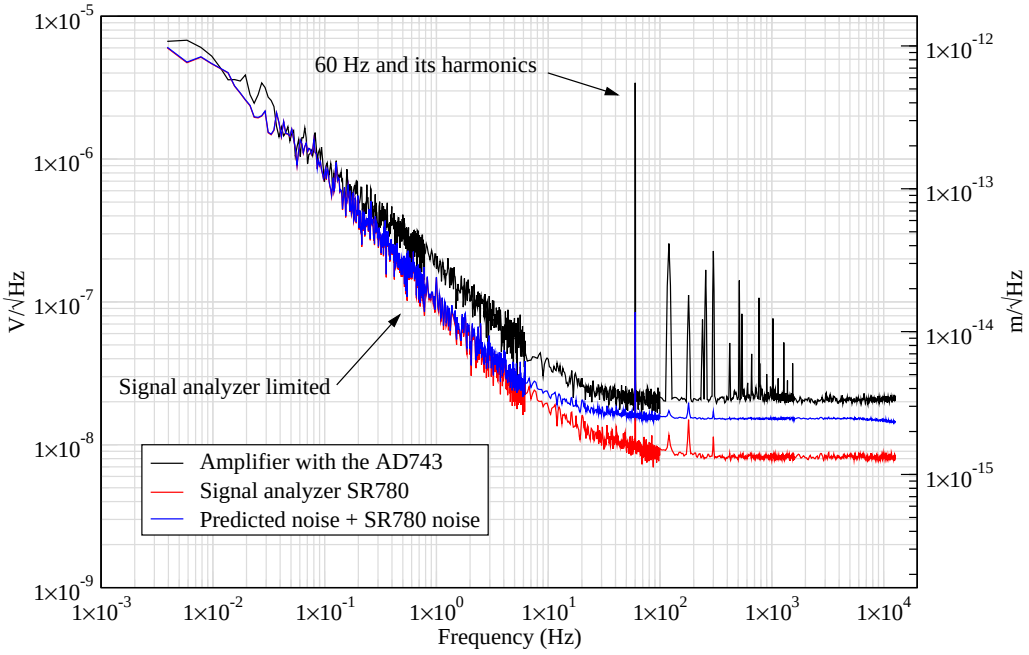

Figure 6: Readout noise produced by the transimpedance amplifier and the photodiode with no incident light. The scale in $m/\sqrt{Hz}$ shown on the right was calculated as it is explained in section V.

variations in the electric field produced by the electrons themselves would affect each other with the consequence of producing $1/f$ noise [2]. The best option would be to apply a low bias voltage. This would decrease the $1/f$ noise at the expense of the dark current flowing through the photodiode and some white noise produced by the shot noise of the dark current.

V. INTERFEROMETER NOISE SOURCES

Figure 7 shows the sensitivity plot of the interferometer. The main identified contributions to the overall noise are ground vibrations and laser intensity noise.

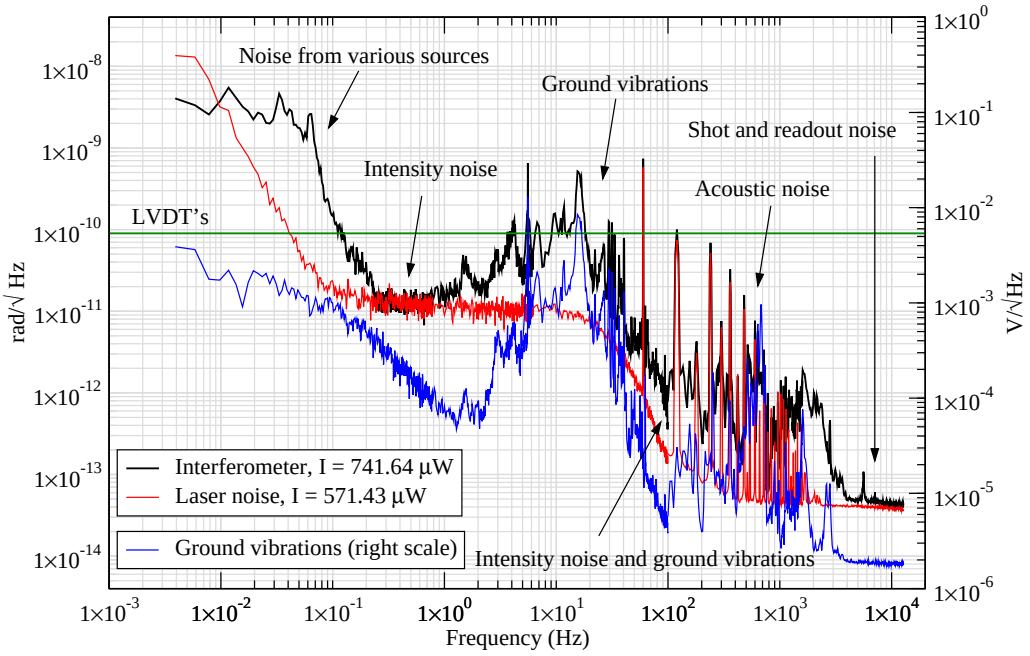

Figure 7: Sensitivity of the interferometer. The scale in $rad/\sqrt{Hz}$ is approximate since the intensity of the interference pattern was not locked. The readout sensitivity of the LVDT's is $9 \times 10^{-11}\, rad/\sqrt{Hz}$.

Before describing each of these noise sources, it is necessary to describe how the measurements were taken with the signal analyzer. In many of the measurements presented in this report, the DC offset of the signal is a lot larger than the amplitude of the noise that is being measured. In those cases it is convenient to use the AC filter provided by the signal analyzer in order to not sacrifice the signal to noise ratio. In the case of low frequency measurements, the transfer function of the filter can be used to calculate the amount of the measured quantity before the attenuation by the filter. Figure 8 shows the transfer function of the filter. It was measured by calculating the ratio of the signals recorded by the two channels

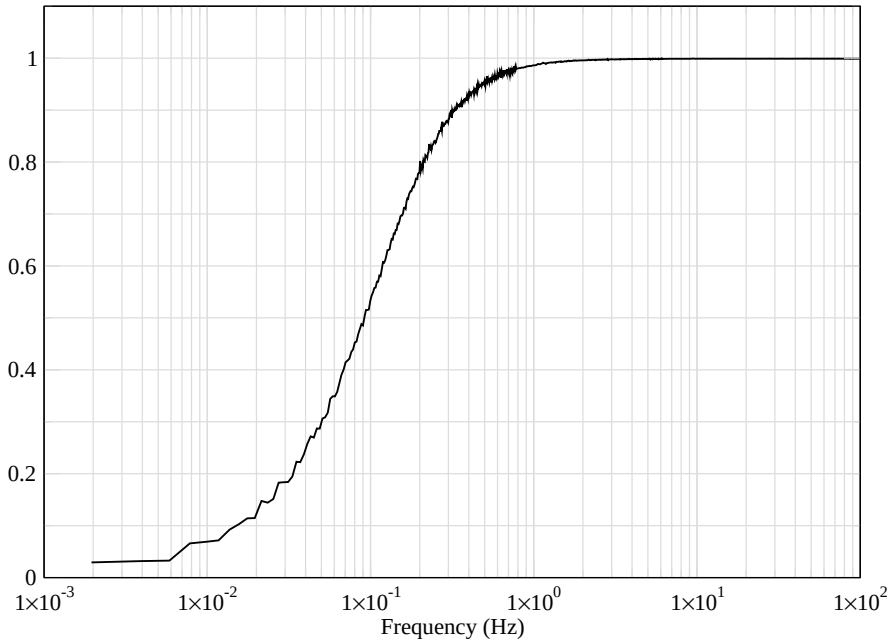

Figure 8: Transfer function of the AC filter in the signal analyzer.

of the signal analyzer, one being DC-coupled and the other AC-coupled, when the same white noise was used as the input voltage.

Another important point to note is that the scales in $rad/\sqrt{Hz}$ given in this report are only approximate since the intensity of the interference pattern was not locked to a constant value. Experimentally, all the measurements that involved the interferometer were made after it was observed, by visual inspection, that the intensity of the pattern remained relatively constant on the oscilloscope screen for an amount of time larger than the time required to complete the measurement. Although this is not equivalent to locking the intensity to a constant value, it does provide an approximate assessment to the real sensitivity of the interferometer. In order to calculate the noise in units of $rad/\sqrt{Hz}$ from the measured noise in terms of $V/\sqrt{Hz}$, it is necessary to consider that the electric signal V_{out} varies

sinusoidally as a function of the phase ϕ

$$V_{out} = V_{dc} + V_{ac} \cos \phi, \tag{20}$$

where V_{dc} and V_{ac} are the offset and amplitude of the signal. The noise in the phase then becomes

$$\sigma(\phi) = \frac{\sigma(V_{out})}{V_{ac} \sin \phi_f}, \tag{21}$$

where ϕ_f is the phase at which the interferometer operates during the measurement. The interferometer was not locked during these measurements, but it simply passively remained at a reasonable constant phase. The sine of such a phase is calculated from expression (20) using the measured values of V_{dc}, V_{ac} and V_{out} when the phase equals ϕ_f. The sensitivity in units of $rad/\sqrt{Hz}$ follows from (21) by writing the angular displacement noise $\sigma(\theta)$ as

$$\sigma(\theta) = \frac{\lambda}{4\pi} \frac{\sigma(\phi)}{l_a}, \tag{22}$$

where the interferometer arm length is $l_a = 250\, mm$. Note that as a consequence of not locking the interference pattern, the low frequency measurements, below $1\, Hz$, should be repeated once the interferometer is locked.

The interferometer was mounted within an open vacuum chamber on a table that provides isolation from vibrations. Figure 9 shows the output of an uncalibrated accelerometer attached to the table as an external periodic disturbance was applied to it. The resonant frequency of the table is approximately 6.6 Hz. Below this frequency no attenuation of ground vibrations is expected.

The laser source used in the interferometer is the linearly polarized helium-neon laser manufactured by $JDSU$ with the part number $1103p$. The light was taken into the interferometer directly from the laser optical cavity. Placing the laser source near the interferometer has the drawback that the heat of the cavity can potentially introduce additional fluctuations in the output signal. The temperature of the laser source remains approximately at $43^{\circ}\, C$. For this reason it is

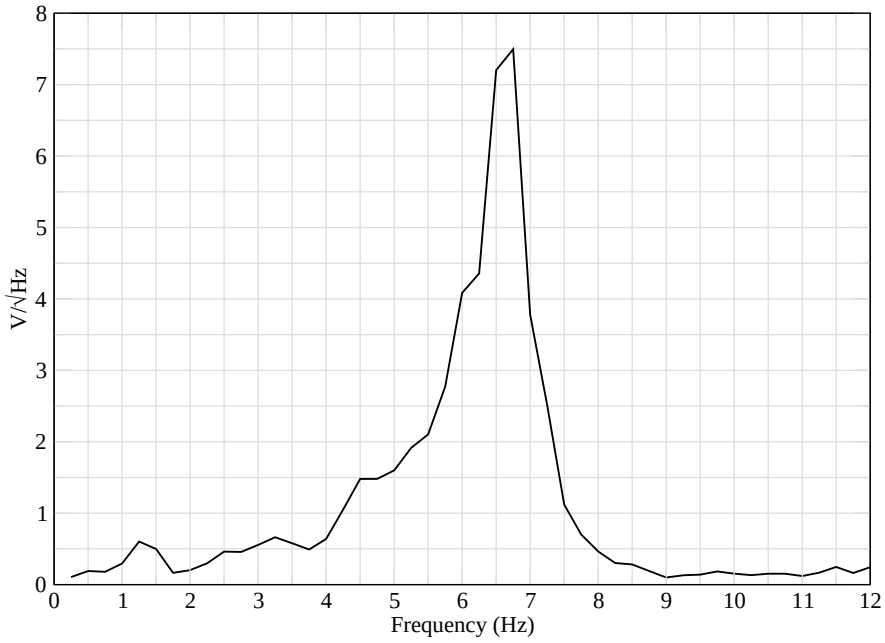

Figure 9: The resonant frequency of the table is approximately 6.6 Hz.

customary to couple the cavity to an optic fibre and keep the cavity away from the interferometer. The fibre is also necessary in order to place the interferometer in vacuum, when needed in later stages of development. However, as will be explained in section V B, the device used to couple the cavity to the fibre does reflect some light into the cavity, yielding the fibre itself very sensitive to ground vibrations, thus increasing the noise affecting the interferometer. In order to use the fibre successfully a Faraday isolator is required between the fibre and the laser cavity.

The intensity of the light produced by the cavity is nominally $4\,mW$. The intensity was reduced using either a neutral density filter, or a polarizing beam splitter while changing the polarization direction of the light by rotating the cavity.

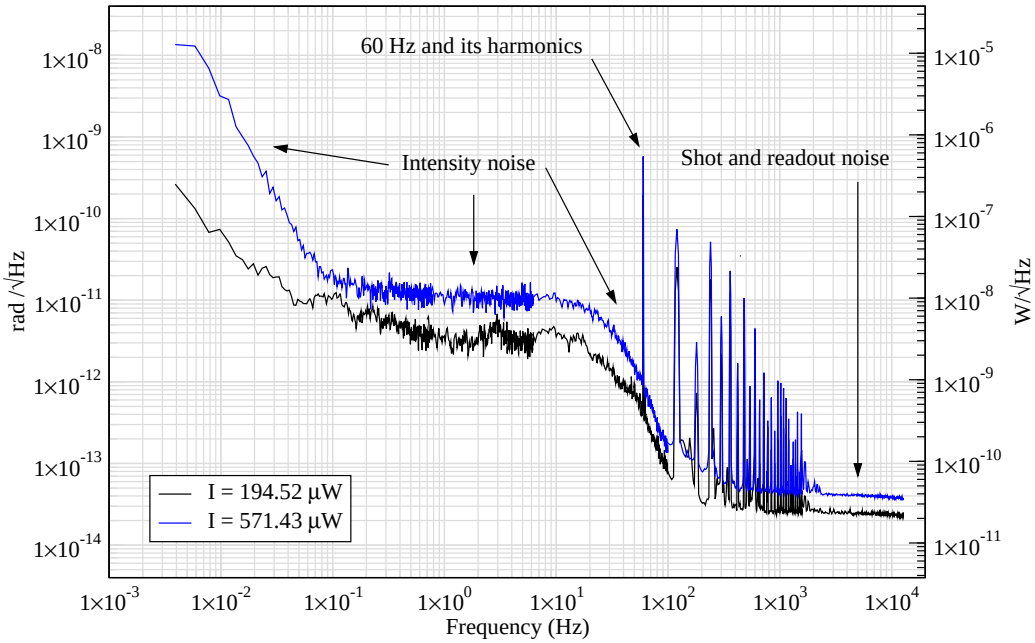

Figure 10: Laser source noise. The noise of the beam with an intensity of $194.52\,\mu W$ is shown in black, the noise of the beam with an intensity of $571.43\,\mu W$ is shown in blue.

A. Laser source noise

The noise present in the laser for two different intensities is shown in figure 10. The curve shown in black was measured by covering one of the arms of the interferometer. The intensity of the incoming beam was measured to be $I = 194.52\,\mu W$. The shot noise produced by the beam is easily calculated as

$$\sigma\left(I\right) = \sqrt{\frac{2qI}{\eta}} = 1.33 \times 10^{-11}\ W/\sqrt{Hz}, \tag{23}$$

where q is the charge of the electron and $\eta = 0.35\,A/W$ is the responsivity of the silicon photodiode at the wavelength of $\lambda = 632.8\,nm$. In order to compare the value (23) with the average measured white noise value of $\sigma_m\left(I\right) = 2.27 \times$

$10^{-11}\ W/\sqrt{Hz}$, shown in figure 10 at frequencies above 3 kHz, it is necessary to also consider the readout noise contribution, which is shown in figure 6. Written in term of light intensity, the average value of the readout white noise $V_{ro} = 2.08\,V/\sqrt{Hz}$ becomes

$$\sigma_{ro} = \frac{V_{ro}}{\eta R_1} = 1.26 \times 10^{-11} \frac{W}{\sqrt{Hz}}, \tag{24}$$

which added to value (23) in quadrature yields the shot noise value of $\sigma_p\,(I) = 1.84 \times 10^{-11}\,W/\sqrt{Hz}$. The difference in quadrature between $\sigma_m\,(I)$ and $\sigma_p\,(I)$ is $1.33 \times 10^{-11}\,W/\sqrt{Hz}$, which, written as a voltage density, becomes $21.9 \times 10^{-9}\,V/\sqrt{Hz}$. Such a difference may have its origin in the different input range settings of the signal analyzer used for taking the measurement in figures 6 and 10. The input range was set to $-50\,dBV$ for the former and $-38\,dBV$ for the latter. Below 1.5 kHz the plot shows peaks at frequencies multiples of 60 Hz associated with the power supply and below 180 Hz the noise is intensity noise.

However, the amount of noise shown in black in figure 10, does not account for all the laser noise affecting the overall sensitivity of the device. In the alignment of the interferometer in which the measurement was taken, the interference pattern was more intense than the beams along any of the two arms. The intensity of the pattern was $741.64\,\mu W$. The curve shown in blue in figure 10 is the noise of a beam with an intensity of $571.43\,\mu W$. Despite it is still not as intense as the interference pattern itself, the corresponding power spectrum does show how the intensity noise contributes to the sensitivity curve shown in figure 7, where it is depicted in red. The calculated shot noise produced by the beam is $2.29 \times 10^{-11}\,W/\sqrt{Hz}$, which added in quadrature to the readout noise (24) yields the value $2.61 \times 10^{-11}\,W/\sqrt{Hz}$. As can be seen in figure 10, the measured value of the noise at frequencies above 3 kHz is $3.71 \times 10^{-11}\,W/\sqrt{Hz}$. The difference between the calculated and measured values is, in units of a voltage, $43.3 \times 10^{-9}\,V/\sqrt{Hz}$. The difference may be due again to the different settings of the input range used for the measurements, but further inquiry is needed.

As can be seen in figure 7, the interferometer noise, shown in black, does follow the trend of the laser noise, shown in red. As will be explained in section V B, in the frequency range from 1 Hz to 4 kHz, the sensitivity is limited by ground vibrations and acoustic noise. However, the sensitivity curve increases as the intensity noise increases suggesting such a contributions is not negligible. Furthermore, as the ground vibration noise decreases, the contribution of the intensity noise begins to dominate between 1 Hz and 200 mHz. Below 200 mHz, despite the intensity noise is not the largest contribution, the noise in the interferometer still follows an increasing trend. Such a trend only suggests that the noise in the interferometer is consistent with the amount of intensity noise in the laser.

For the sensitivity curve of the interferometer, the intensity of the interference pattern was measured to be approximately $I_{int} = 741.64\,\mu W$. The maximum and minimum intensities of the interference pattern were $I_{max} = 790.27\,\mu W$ and $I_{min} = 3.16\,\mu W$ respectively. In units of displacement, the calculated shot noise density produced by the interference pattern at the intensity I_{int} is $2.77 \times 10^{-14}\,rad/\sqrt{Hz}$, which, added in quadrature to the readout noise, yields the calculated value of $3.08 \times 10^{-14}\,rad/\sqrt{Hz}$. The average of the measured value of the noise above 3 kHz is $4.92 \times 10^{-14}\,rad/\sqrt{Hz}$. The difference in quadrature, in units of voltage, is $59.67 \times 10^{-9}\,V/\sqrt{Hz}$. The difference may be due again to the different settings of the input range used for the measurements.

It is important to note that with the laser source used, the more intense the beam is, the larger the intensity noise becomes. According to expression (21), the advantage of using an intense beam (large V_{ac}) is that the noise $\sigma(V_{out})$ in the measured output signal V_{out} attenuates as it is propagated into phase noise $\sigma(\phi)$. In the case of the intensity noise, this propagated effect appears as the relative intensity noise. This quantity is defined as the intensity noise divided by the average intensity. The optimal sensitivity then becomes a compromise between the relative intensity noise and the increasing resolution that a large amplitude of the

interference pattern implies. An approach that may remove the relative intensity noise, would be to measure the intensity of a sample of the initial incoming beam and use it to normalize the output signal of the interferometer. Another approach would be to stabilize the intensity with a feedback control system.

B. Ground vibrations

The most important contribution to the overall noise in the interferometer are the ground vibrations and acoustic noise. Figure 11 shows the sensitivity of the interferometer together with the power spectral density of the ground vibrations measured with an accelerometer, for two values of the intensity of the interference pattern (a) $I = 741.64\,\mu W$ and (b) $I = 13.71\,\mu W$. The scale quantifying the ground vibrations has been shifted arbitrarily for best image overlap in order to point out the effect of the vibrations upon the overall sensitivity. From $2\,kHz$ down to $1\,Hz$, many of the features of the noise are shared by both the interferometer and the accelerometer. Two exceptions can be noticed in plot (a), at frequencies below 6 Hz down to $200\,mHz$ and in the vicinity of 100 Hz, where the intensity noise contribution is also important. In plot (b), in which the intensity of the interference pattern is a lot lower and the intensity noise is not as high, the noise in the interferometer is almost completely dominated by the ground vibrations. The comparison between plots (a) and (b) points out the fact that the larger the intensity is, the larger the intensity noise becomes. However, as pointed out above in section V A, a meaningful comparison between these quantities can only be achieved in terms of their respective relative intensity noise contributions. Above 200 Hz there is acoustic noise. Below 200 mHz, the dominant noise source is likely to be ground vibrations since no attenuation is expected from the supporting table below its resonant frequency at 6.6 Hz. Nevertheless, noise from other sources like mechanical drift of the assembly, air density fluctuations and laser frequency drift

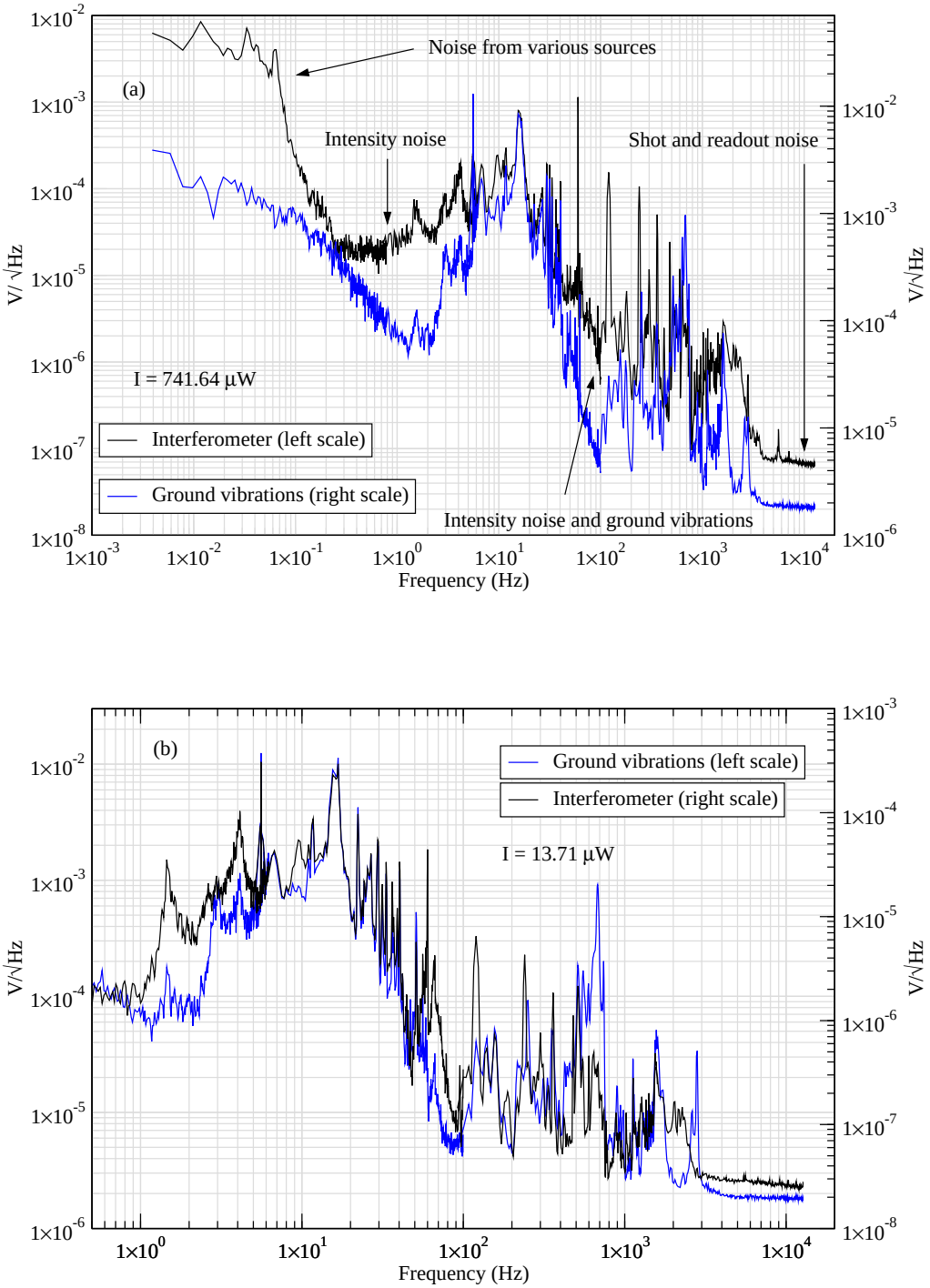

Figure 11: Between 4 Hz and 2 kHz the interferometer is limited by ground vibrations. In plot (a) the intensity of the interference is 741.64 μW and below 4 Hz, what is likely actual displacement noise begins to dominate. Other noise sources in the interferometer are also pointed out. In (b) the intensity is only 13 μW and the intensity noise is not as high.

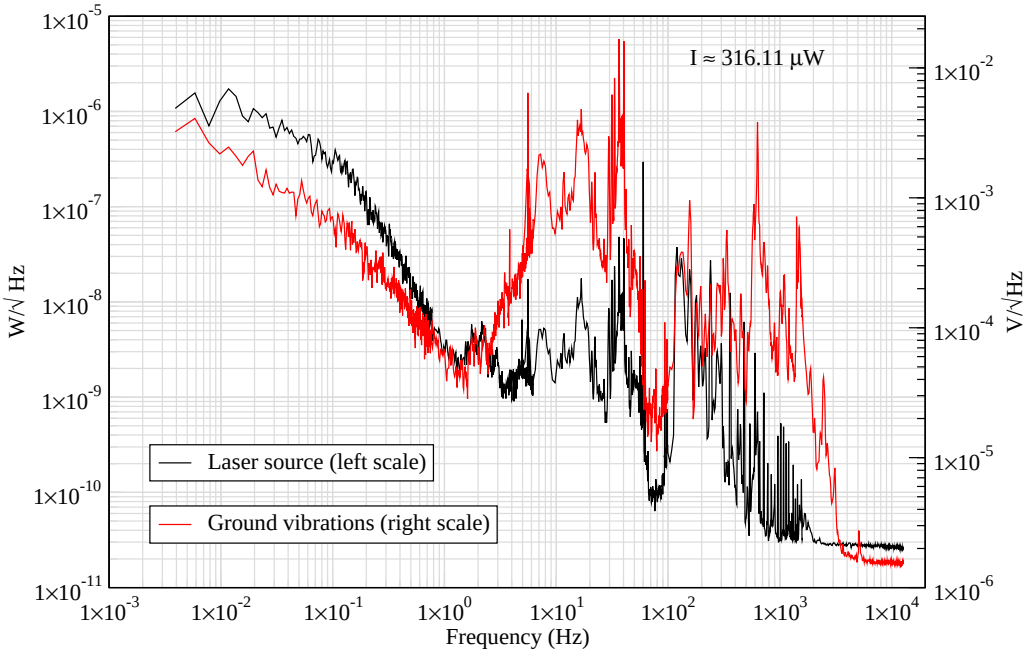

Figure 12: When the optic fibre is used, the intensity is coupled to the ground vibrations.

is likely to be present at this frequency range also, but further inquiry would be necessary in order to estimate the extent of each contribution.

Although it is clearly a goal of the mechanical system to minimize vibration noise, the effect that these have in the intensity of the laser is useful for assessing the effect of feedback light into the laser cavity. For instance, figure 12 shows the noise measured when a single mode fibre was used to take the light from the laser cavity into the optical system. One of the arms of the interferometer was covered in order to take this measurement. The intensity of the light was 316.11 μW. Above 2 kHz the dominant source is shot noise with a value of $2.88 \times 10^{-11}\ W/\sqrt{Hz}$. Bellow 2 kHz it is possible to notice the peaks at frequencies multiples of 60 Hz. Bellow 500 Hz acoustic noise and ground vibrations dominate. The sensitivity of the fibre is likely caused by feedback light into the laser cavity from the system

used to couple the cavity to the fibre. Such a system is an xyz translation stage that finely adjusts the position of a microscope objective in order to place the focal point of the light into the core of the optic fibre. By visual inspection it is clear that there is a large amount of light being reflected back into the cavity. A Faraday isolator between the xyz translation stage and the laser cavity would be an appropriate solution for this issue.

In the case in which the laser was taken into the interferometer directly from the optical cavity, the folding mirrors were adjusted in such a way that no light from the interferometer went back into the cavity and, therefore, no large coupling between the laser intensity noise and ground vibrations is expected. There can be residual light going into the laser cavity due to stray reflections, although it was not detected by visual inspection. Using a Faraday isolator would avoid any feedback of stray light, with the possible effect of decreasing the noise at low frequencies below 200 mHz.

VI. CONCLUSIONS AND FUTURE WORK

As can be seen in figure 7, the interferometer is limited by different noise sources in different frequency regimes. These noise sources are actual displacement noise, laser intensity noise, ground vibrations and acoustic noise. The noise floor level of $4.5 \times 10^{-14}\, rad/\sqrt{Hz}$ is determined by laser shot noise and readout noise produced by the signal analyzer used to take the measurement.

The interferometer is a device that potentially has a much better resolution that, for instance, the LVDT's or capacitive sensors. However, its usage is more complex and is justified only in measurements that require better precision. As pointed out in the introduction, the interferometer is a tool to improve the performance of the tiltmeter by analyzing advanced knife edges and the elastic properties of new materials rather than a substitute of the LDVT's as the default readout.

The future work include various strategies that aim to reduce the amount of noise in the system. The implementation of a feedback loop to lock the interferometer intensity to a certain value would avoid any variation in the conversion factor (21) that would be translated as noise in the final estimate of the phase. Such a loop has already been experimentally implemented with success by Emanuele Sobacchi [3]. The effect of the laser intensity noise can also be reduced by normalizing the intensity of the interference pattern with the intensity of a sample of the incoming beam into the interferometer, or by stabilizing the laser power. As pointed out in section V B a Faraday isolator is needed in order to avoid any feedback light into the laser cavity and thus further reduce the effects of ground vibrations. The Faraday isolator would also aid in successfully coupling an optic fibre to the laser cavity while avoiding any feedback from the stray reflections coming from the xyz translation stage used to couple the fibre to the cavity. The use of a fibre is convenient in order to place the laser cavity far away from the interferometer since it is a source of heat that may introduce low frequency noise. The interferometer must also be placed in vacuum, for which the fibre is also required. In vacuum, the acoustic noise and any possible disturbance of air currents would disappear. Using a quiet table with a lower frequency resonance would also improve the performance. Finally, the interferometer must be mounted on the tiltmeter.

---

[1] Vladimir Dergachev. Personal communication, 2010.

[2] Riccardo De Salvo. Personal communication, 2010.

[3] Emanuele Sobacchi. Personal communication, 2010.

[4] Thorlabs Inc. `http://www.thorlabs.com/newgrouppage9.cfm?objectgroup_id=2970`.